JPL NO. 9950-314

DOE/JPL-954685-80/3
Dist. Category UC-63

STUDY OF THE EFFECTS OF IMPURITIES ON THE PROPERTIES OF SILICON MATERIALS AND PERFORMANCE OF SILICON SOLAR CELL

THIRD TECHNICAL REPORT

(NASA-CR-162626) STUDY OF THE EFFECTS OF IMPURITIES ON THE PROPERTIES OF SILICON MATERIALS AND PERFORMANCE OF SILICON SOLAR CELL (Jet Propulsion Lab.) 37 p HC A03/MF A01 CSCL 10A G3/44 N80-21832 Unclas 46748

February 1980

By C. T. Sah

Contract No. 954685

The JPL Low Cost Solar Array Project is sponsered by the U. S. Dept. of Energy and forms a part of the Solar Photovoltaic Conversion Program to initiate a major effort toward the development of low-cost solar arrays. This work was performed for the Jet Propulsion Laboratory, California Institute of Technology by agreement between NASA and DOE.

DOE/JPL-954685-80/1
Dist. Category UC-63

STUDY OF THE EFFECTS OF IMPURITIES ON THE PROPERTIES OF SILICON MATERIALS AND PERFORMANCE OF SILICON SOLAR CELL

THIRD TECHNICAL REPORT

February 1980

By C. T. Sah

Contract No. 954685

The JPL Low Cost Solar Array Project is sponsered by the U. S. Dept. of Energy and forms a part of the Solar Photovoltaic Conversion Program to initiate a major effort toward the development of low-cost solar arrays. This work was performed for the Jet Propulsion Laboratory, California Institute of Technology by agreement between NASA and DOE.

TECHNICAL CONTENT STATEMENT

This report was prepared as an account of work sponsered by the United States Government. Neither the United States nor the United States Department of Energy, nor any of their employees, nor any of their contractors, sub-contractors, or their employees, makes any warranties, express or implied, or assumes any legal liability or responsibility for the accuracy, completeness or usefulness of any information, apparatus, product or process disclosed, or represents that its use would not infringe privately owned rights.

NEW TECHNOLOGY

No new technology is reportable for the period covered by this report.

TABLE OF CONTENT

Section		Page
	TECHNICAL CONTENT STATEMENT	i
	NEW TECHNOLOGY STATEMENT	ii
	TABLE OF CONTENT	iii
	LIST OF FIGURES	iv
	LIST OF TABLES	v
	ABSTRACT	1
I.	INTRODUCTION	2
II.	EFFECT OF ZINC IMPURITY ON SILICON SOLAR CELL EFFICIENCY	3
	1. INTRODUCTION	3
	2. RECOMBINATION PROPERTIES OF ZINC CENTERS IN SILICON	3
	2.1 First Acceptor Level (E_V + 326 meV)	5
	(A) Thermal Hole Capture Rate, c_{p1}	5
	(B) Thermal Electron Capture Rate, c_{n0}	7
	(C) Thermal Hole Emission Rate, e_{p0}	9
	(D) Thermal Electron Emission Rate, e_{n1}	9
	2.2 Second Acceptor Level (E_V + 664 meV)	10
	(A) Thermal Hole Capture Rate, c_{p2}	10
	(B) Thermal Electron Capture Rate, c_{n1}	10
	(C) Thermal Hole Emission Rate, e_{p1}	11
	(D) Thermal Electron Emission Rate, e_{n2}	11
	3. THEORETICAL AND COMPUTER MODEL	12
	4. PROJECTED AM1 PERFORMANCE	16
	5. CONCLUSIONS	20
	APPENDIX	21
	REFERENCES	28

LIST OF FIGURES

Figure Number		Page Number

1. Computer plot of sampled voltage stimulated capacitance transients (VSCAP) as a function of diode temperature of a zinc-diffused silicon n+/p diode. The two peaks are from thermal emission of holes trapped at the two zinc acceptor levels, E_V+326 and E_V+664 meV above the valence band edge of silicon. 4

2. Theoretical AM1 efficiency as a function of Zn concentration at 296.6K for bcak surface field silicon solar cells with perfect antireflection coating. Curves 1a and 2a include interband Auger recombination. Curves 1 and 1a are for n+/p/p+ and curves 2 and 2a are for p+/n/n+ cells. 17

3. Theoretical AM1 open circuit voltage as a function of Zn concentration at 296.6K for back surface field silicon solar cells with perfect antireflection coating. Solid curves are for n+/p/p+ cells and dashed curves p+/n/n+ cells. Curves labeled 'a' include interband Auger recombination. 18

4. Theoretical AM1 short circuit current as a function of Zn concentration at 296.6K for back surface field silicon solar cells with perfect antireflection coating. Solid curves are for n+/p/p+ cells and dashed curves p+/n/n+ cells. Curves labeled 'a' include interband Auger recombination. 19

LIST OF TABLES

Table Number		Page Number
1.	The thermal emission and capture rates at the double acceptor zinc centers in silicon at room temperature	6
2.	AM1 solar spectral irradiance, P, silicon absorption coefficient, α, and silicon surface reflection coefficient, $R(\lambda)$, as a function of photon wave length, λ. The total incident power is 88.92 mW/cm^2.	
	(Part 1, 2900-6000A)	22
	(Part 2, 6000-12640A)	23

ABSTRACT

Zinc is a major residue impurity in the preparation of solar grade silicon ma' rial by the zinc vapor reduction of silicon tetrachloride. This paper projects that in order to get a 17% AM1 cell efficiency for the Block IV module of the Low-Cost Solar Array Project*, the concentration of the zinc recombination centers in the base region of silicon solar cells must be less than 4×10^{11} Zn/cm^3 in the p-base n+/p/p+ cell and 7×10^{11} Zn/cm^3 in the n-base p+/n/n+ cell for a base dopant impurity concentration of 5×10^{14} atoms/cm^3. If the base dopant impurity concentration is increased by a factor of 10 to 5×10^{15} atoms/cm^3, then the maximum allowable zinc concentration is increased by a factor of about two for a 17% AM1 efficiency. The thermal equilibrium electron and hole recombination and generation rates at the double acceptor zinc centers are obtained from previous high field measurements as well as new measurements at zero field described in this paper. These rates are used in the exact d.c. circuit model to compute the projections.

---

*See for example JPL/DOE 5101-143 p.21, a report distributed at the 14th Photovoltaic Specialist Conference, January 1980.

I. INTRODUCTION

The objective of this program is to determine the effects of impurities and defects on the performance and permanence of silicon solar cells. It includes theoretical (computer model) and experimental studies of the effects of impurities on the properties of silicon intentionally doped with specific impurity elements, as well as the effects of these impurities on the impurity related energy level positions, the concentration of these energy levels and the recombination-generation properties of electrons and holes at these energy levels.

This third technical report contains a theoretical projection of the maximum level of zinc recombination centers in silicon which is allowable to give a AM1 silicon solar cell efficiency of 17%.

The thermal recombination and generation rates of electrons and holes at the double acceptor zinc centers in silicon are obtained from published results in the literature as well as new measurements described in this report. These values, considered to be the currently best values at 300K, are used in the transmission line equivalent circuit model to compute the performance of silicon p+/n/n+ and n+/p/p+ cells doped with zinc from 10^{10} to 10^{14} Zn/cm^3.

Chapter II gives a detailed description of the zinc recombination and generation rate data, the material and device parameters used in the theoretical computation, and the performance of the silicon solar cells computed using the one-dimensional exact equivalent circuit model and these parameters. The AM1 solar spectral density, the silicon absorption coefficient and silicon surface reflection coefficient are tabulated in the appendix. The silicon properties, the intrinsic carrier concentration and the electron and hole mobilities, used in the theoretical computation are also given in the appendix.

II. EFFECT OF ZINC IMPURITY ON SILICON SOLAR CELL EFFICIENCY

1. INTRODUCTION

In producing low cost silicon stock by zinc vapor reduction of silicon tetrachloride in a fluidized bed, a large amount of zinc impurity remains in the granular silicon product [1]. The residue zinc will give high concentrations of zinc recombination centers in single crystals or sheets grown using this zinc reduced silicon stock. This analysis provides a guideline on the maximum amount of zinc allowable in a silicon solar cell fabricated from such a single silicon crystal or sheet for a desired AM1 energy conversion efficiency.

2. RECOMBINATION PROPERTIES OF ZINC CENTERS IN SILICON

Zinc is a double acceptor in silicon [2,3]. The first acceptor level is located at 326 meV above the silicon valence band edge and the second acceptor level is located at 664 meV above the silicon valence band edge. These were determined by Herman [4,5] using the transient capacitance and current methods [6,7,8]. Strong and nearly equal-amplitude voltage stimulated capacitance transient (VSCAP) [8] and thermally-stimulated capacitance (TSCAP) [9] signals are observed due to thermal emission of holes trapped at these two levels. The VSCAP peaks are illustrated in Figure 1

Detailed and extensive measurements of the thermal capture and emission rates of electrons and holes at these zinc levels have been made by Herman [4,5] in diffused silicon p+/n and n+/p diodes which were also zinc diffused in a closed quartz ampoule. However, these measurements were made at high electric fields in reverse biased p/n junctions. In order to predict the performance of silicon solar cells containing zinc, recombination rates at low or zero electric fields are needed. Some of the high field data can be extrapolated to low

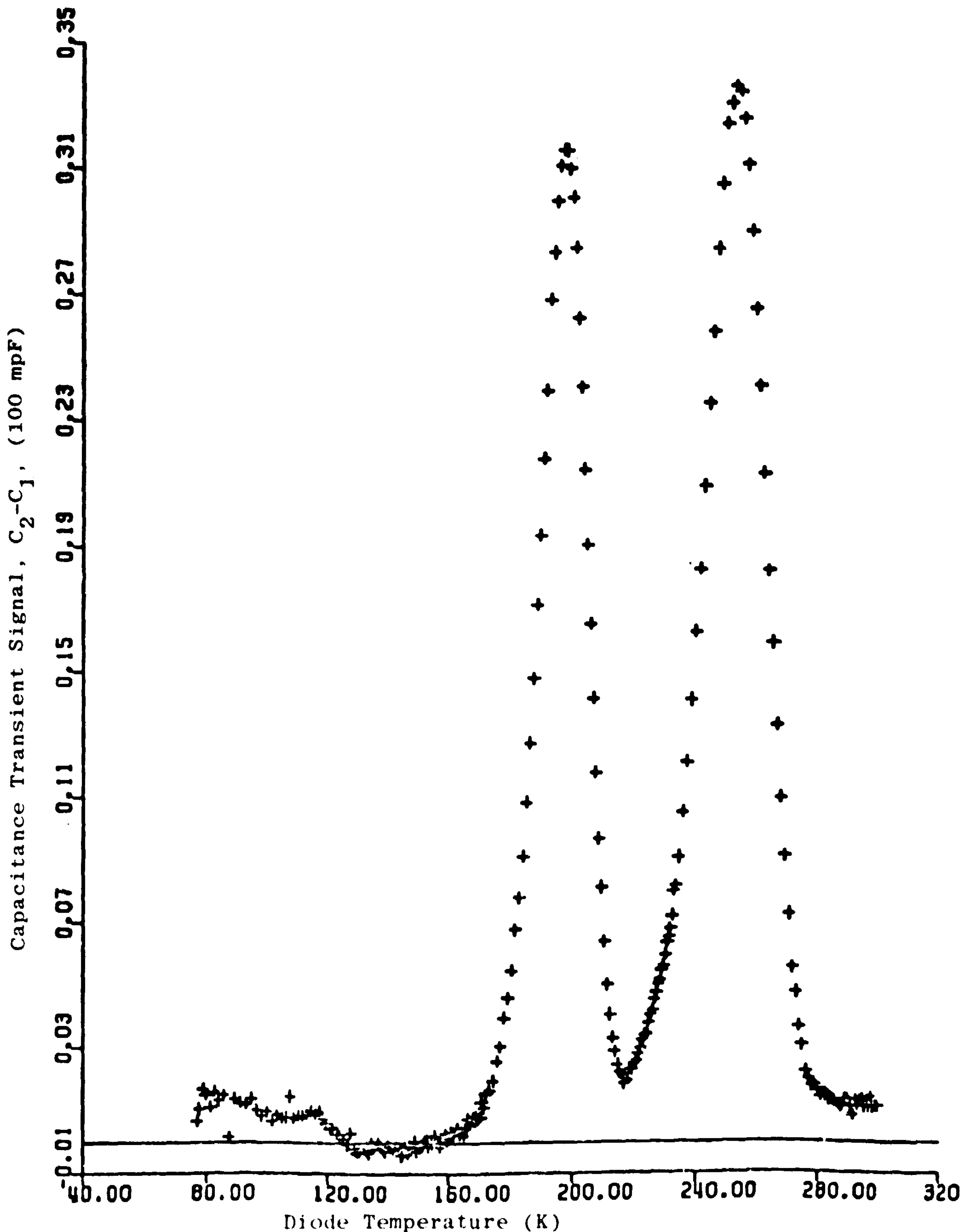

Figure 1 Computer plot of sampled voltage stimulated capacitance (VSCAP) as a function of diode temperature of a zinc-diffused silicon n+/p diffused diode. The two peaks are from thermal emission of holes trapped at the two zinc acceptor levels, E_v+326 and E_v+664 meV above the valence band edge of silicon.

fields but additional low field data are still needed to give sufficiently accurate thermal capture rates of electrons and holes at the zinc levels at low fields in order to predict the solar cell performance. These were made and the results of the thermal capture and emission rates at the two zinc acceptor levels are listed in Table 1 and compared with those values used in a recent study of the dark forward current-voltage (I-V) characteristics of zinc doped silicon diodes. [10] The methods by which these new values were obtained are discussed in the following two subsections.

2.1 FIRST ACCEPTOR LEVEL (E_V + 326 meV)

The thermal recombination kinetics at this level are characterized by the two capture rates, c_{p1} and c_{n0}, and the two emission rates, e_{p0} and e_{n1}. The numeral subscript, 0 or 1, indicates the number of electrons trapped at the zinc center *prior* to the indicated electron or hole transition [11]. The reference state, subscript 0, is the electrically neutral charge state. Thus, c_{p1} is the capture rate of holes by a negatively charged zinc center. The determination of their values at room temperature, 23.4C or 296.6K, is described for each of the rate constant given below. The temperature 296.6K is used here since it corresponds to a convenient value of the intrinsic carrier density of $n_i = 1.000 \times 10^{10}$ carriers/cm^3.

(A) Thermal Hole Capture Rate, c_{p1}.

The thermal hole capture rates at singly negatively charged zinc center, c_{p1}, were measured by Herman [5] at 83K as a function of the electric field from 2.5×10^4 to 10^5 V/cm. This is extrapolated to give a zero field value of $(4 \pm 2) \times 10^{-7}$ cm^3/sec. Zero field capture rates were also measured by us using the voltage stimulated capacitance transient (VSCAP) [8] at 112.57 and 122.7K with values of 3.6×10^{-7} and 3.9×10^{-7} cm^3/sec respectively.

Table 1

The Thermal Emission and Capture Rates at the Double Acceptor Zinc Centers in Silicon at Room Temperature

Energy Level = E_V + 664 meV

Rates	This Work 296.6K	Dark I-V[a] 297.0K	Sources
c_{n1} (cm^3/s)	$2x10^{-12}$	$5x10^{-11}$	Exp.
e_{n2} (1/s)	0.41	11	Computed
c_{p2} (cm^3/s)	$6x10^{-8}$	$6x10^{-8}$	Exp.
e_{p1} (1/s)	29	29	Exp.

Energy Level = E_V + 326 meV

Rates	This Work 296.6K	Dark I-V[a] 297.0K	Sources
c_{n0} (cm^3/s)	$2x10^{-8}$	$2x10^{-9}$	Exp.
e_{n1} (1/s)	$5x10^{-3}$	$9x10^{-3}$	Computed
c_{p1} (cm^3/s)	$5x10^{-8}$	$9x10^{-8}$	Exp.
e_{p0} (1/s)	$2x10^{7}$	$2x10^{7}$	Exp.

[a] Rate data from reference 10.

In our recent study of the dark forward I-V characteristics of zinc diffused silicon diodes [10], it was assumed that c_{p1} was independent of temperature so that the 83K value of Herman just quoted was used at room temperatures. Although the new values obtained from direct capture rate measurements at 123K showed that the capture rates are nearly constant from 83 to 123K, we prefer an extrapolation to 296.6K be made by following the temperature dependence of the c_{p2} capture rate since in principle we expect $c_{p1} < c_{p2}$. If c_{p1} were taken to be constant, then at 296K, we would have $c_{p1} > c_{p2}$ while the experimental data at $T < 125K$ showed $c_{p1} < c_{p2}$. The sources of c_{p2} data are described in the next subsection.

This extrapolation gives a value of $c_{p1}=5x10^{-8}$ cm^3/sec at 296.6K which is two (2) times smaller than the previous value of $9x10^{-8}$ cm^3/sec [10].

(B) Thermal Electron Capture Rate, c_{n0}

The thermal electron capture rates at the neutral zinc center, c_{n0}, were measured by us recently using the diode forward-injection-reverse-recovery method [12] since the VSCAP experiment cannot set the initial charge states of the zinc centers to the neutral charge state to observe this electron transition. The use of this diode current recovery method requires a careful interpretation of the result based on the recombination kinetics of a double acceptor level. The necessary theoretical model was given previously [13]. The high level lifetime at the experimental forward injection current of 10 mA or 1200 mA/cm^2 had a nearly constant value of 633 ns in a zinc diffused p+/n diode and 643 ns in a zinc diffused n+/p diode. The diodes used in these experiments were those fabricated by Herman [4]. The nearly constant and equal high level lifetimes in the n-type and p-type bases are consistent with the theoretical considerations which lead to the conclusion that electron capture by the neutral zinc center should be the dominant recombination transition which controls the high level

lifetime in the base region. This is arrived at as follows. From the two-level theory [13], the high level steady-state lifetime or transient lifetime is given by

$$\tau_H = (c_{n0}c_{n1} + c_{n0}c_{p2} + c_{p1}c_{p2})/[c_{n0}c_{p2}(c_{p1} + c_{n1})N_{TT}] \qquad (1)$$

In general, we would expect $c_{n1} \ll c_{p1}$ and $c_{n1} \ll c_{p2}$ since c_{n1} is associated with a repulsive potential from the singly negatively charged zinc center while both c_{p1} and c_{p2} are associated with attractive potentials from singly and doubly negatively charged zinc centers. The experimental data of c_{n1} described in the next subsection indeed confirms these inequalities. Thus, the high level lifetime given by Equation (1) simplifies to

$$\tau_H \simeq (c_{n0} + c_{p1})/c_{n0}c_{p1} \equiv \tau_{n0} + \tau_{p1} \qquad (2)$$

where $\tau_{n0} \simeq 1/c_{n0}N_{TT}$ and $\tau_{p1} \simeq 1/c_{p1}N_{TT}$.

The simplified result given by Equation (2) shows that the high level recombination lifetime in a quasi-neutral base region is nearly entirely determined by the recombination through the lower or first acceptor level. This result is quite general and it also applies to a double donor center such as sulfur in silicon. However, it is generally not applicable to a two-level amphoteric impurity such as gold which has a donor and an acceptor level in silicon, except for special circumstances. For the amphoteric center, we have no assurance that one of the capture rates is substantially smaller than the other three, however, the case of gold is close to this situation, making the lower gold donor level the dominant recombination level at high injection levels.

For the first zinc acceptor level considered in this section, the zinc concentration in the diodes is $N_{TT}=10^{14}$ Zn/cm^3 whose maximum value may be as high as 1.7×10^{14} Zn/cm^3 at the junction due to pile up and enhanced solubility in the phosphorus diffused n+ emitter layer. Using the smaller and bulk value,

and $c_{p1}=5\times10^{-8}$ cm^3/sec just obtained in section (A), the electron capture rate at the neutral zinc center is

$$c_{n0} = 1/\tau_{n0}N_{TT} \simeq 1/(\tau_H - \tau_{p1})N_{TT}$$

$$= 1/(643-200)\times10^{-9}\times10^{14} = 2.25\times10^{-8} \text{ cm}^3/\text{sec} \qquad (3)$$

This is ten ([illegible])) times larger than the previously used value of 2×10^{-9} cm^3/sec [10]. It would increase the efficiency reduction in n-based silicon solar cell by the presence of zinc.

(C) Thermal Hole Emission Rate, e_{p0}

The thermal hole mission rate, e_{p0}, is computed from the experimental Arrhenius equation obtained by Herman at low temperatures [4],

$$e_{p0} = 7.4\times10^{12}(T/300)^{-1} \exp(-326/kT) \qquad (4)$$

where k=0.08617087 meV/K. Herman found a large electric field dependence of this hole thermal emission rate. The T^{-1} dependence of the pre-exponential or collision frequency factor is selected since $c_{p1} \propto T^{-2.5}$ so $c_{p1}N_V \propto T^{-2.5}T^{1.5} = T^{-1}$. A different temperature exponent, such as T^{-2}, will change e_{p0} by less than a factor of 2. However, the magnitude of e_{p0}, if varied by a factor of 2 or even more, will have little effect on the predicted solar cell performance since it depends mainly on the capture rates and not the emission rates. The value computed from Equation (4) is 2.2×10^7 1/sec at 297K and about 2×10^7 1/sec at 296.6K which is used in this work.

(D) Thermal Electron Emission Rate, e_{n1}

The thermal electron emission rate from the negatively charged zinc center is computed from the mass action law at thermal equilibrium since under forward bias, the quasi-neutral base region of a solar cell is nearly at thermal equilibrium. The mass action law is $e_{n1}e_{p0}/c_{n0}c_{p1} = n_i^2$. Using $n_i=1.0\times10^{10}$ cm^{-3} at 296.6K, we have $e_{n1} = 5\times10^{-3}$ 1/sec.

2.2 SECOND ACCEPTOR LEVEL (E_V + 664 meV)

The thermal recombination kinetics at this level are characterized by the two capture rates, c_{p2} and c_{n1}, and the two emission rates, e_{p1} and e_{n2}.

(A) Thermal Hole Capture Rate, c_{p2}

A low field value of $6x10^{-8}$ cm^3/sec is extrapolated from Herman's high field data at three temperatures [5], $1.4x10^{-6}$ at 135K, $7.5x10^{-7}$ at 159K, and $3.0x10^{-7}$ at 190K. This is the same extrapolated value used by us previously in diode dark current-voltage characteristics studies [10].

(B) Thermal Electron Capture Rate, c_{n1}

This electron capture rate is expected to be very small since the electron is captured into a repulsive impurity potential of the negatively charged zinc center. The previous values were obtained by Herman [5] at low temperatures and in high electric fields,$(1-8)x10^4$ V/cm. His values were $4.6x10^{-11}$ cm^3/sec at 138K, $4.4x10^{-11}$ cm^3/sec at 150K, $5.2x10^{-11}$ cm^3/sec at 165K and $1.1x10^{-11}$ cm^3/sec at 181K. Since the capture is by a repulsive potential well, we would expect the capture rate to be highly dependent on the electric field. At lower fields, the impurity potential barrier would not be lowered as much and the capture rate should be substantially reduced from the high field value. Thus, new measurements of the thermal equilibrium capture rates were made by us using the VSCAP method [8]. Data were obtained at three temperatures, giving $4x10^{-13}$ cm^3/sec at 230K, $6.2x10^{-13}$ cm^3/sec at 250K and $1.1x10^{-12}$ cm^3/sec at 270K. These data can be fitted to the Arrhenius equation since the repulsive potential well gives rise to a thermally activated process. The result is

$$c_{n1} = (3.7 \pm 2.8)x10^{-10}\exp[-(136\pm16)/kT] \quad cm^3/sec \qquad (5)$$

Extrapolating to 296.6K gives a value of $2x10^{-12}$ cm^3/sec.

This thermal equilibrium value is twenty-five (25) times smaller than the high field value at low temperatures previously used, $5x10^{-11}$ cm^3/sec. The large

high field value at low temperatures is probably due to the lowering of the repulsive potential barrier by the high electric field. At low fields, the barrier height is about 136 meV as deduced by the thermal activation energy of the electron capture rate given by Equation (5).

(C) Thermal Hole Emission Rate, e_{p1}.

The thermal hole emission rate from the singly negatively charged zinc center, e_{p1}, is again obtained from the experimental Arrhenius equation obtained by Herman at low temperatures [4],

$$e_{p1} = 5.36\times10^{12}(T/300)^{-2}\exp(-664/kT) \tag{6}$$

who found essentially no electric field dependences from 10^4 to 10^5 V/cm and in the range of 200 to 360K. The T^{-2} depenaence is selected here since $c_{p2} \propto T^4$, however, a different power will change e_{p1} by only a few percent which would have no effect on the recombination rate under solar cell operating conditions. At 297K, Equation (6) gives e_{p1}=28.94 1/sec. If the T^{-1} dependence is used with ΔE=641 meV, then e_{p1}=28.64 1/sec which differs very little from 28.94 given by Equation (6).

(D) Thermal Electron Emission Rate, e_{n2}

The thermal electron emission rate at the doubly negatively charged zinc center is computed from the mass action law, $e_{n2}e_{p1} = c_{n1}c_{p2}n_i^2$ which gives $e_{n2} = 0.41\ \mathrm{sec}^{-1}$.

3. THEORETICAL AND COMPUTER MODEL

The performance of silicon solar cells was computed by numerically solving the six Shockley Equations for two-level recombination centers [14]. A 198 lump section transmission line equivalent circuit model was synthesized from these equations [13,15]. A photocurrent generator was added to each of the lump sections to represent the solar illumination. Numerical solutions of the quasi-Fermi potentials for electrons and holes and the electrostatic potential at each of the 198 sections were obtained by standard circuit analysis technique involving the diagonization of a 198x3 sparse matrix. Infinite interface recombination at the front and back surfaces were simulated by short-circuiting the three potential nodes at each of the two interfaces. The solution procedure began by assuming a distribution of the electrostatic potential at equilibrium (zero applied voltage in the dark) where the quasi-Fermi potentials have a constant value. The errors of this initial guess of the electrostatic potential were computed from the small-error transmission line circuit model and added to the initial guess to get a new set of 198 electrostatic potentials. This iteration procedure was continued until a specified accuracy was reached by all 198 electrostatic potentials.

In the next step, a small photocurrent generator was added between the electron and hole quasi-Fermi potential nodes at each of the 198 positions while the applied voltage was kept at zero. The converged dark solution of the electrostatic potentials just obtained were used as the initial guess. The interation procedure was then repeated to get the converged solutions of the three potentials at each of the 198 positions. The photocurrent generator was then increased and the iteration calculation repeated until the illumination reached the AM1 intensity, giving the AM1 short-circuit solutions. Then, the applied voltage was stepped in 50 mV increments and the iteration repeated until an applied voltage where the computed diode current changed sign. At this point, the solution had passed the open-circuit condition and the iteration was stopped.

The accurate maximum power efficiency and open circuit voltage were obtained by a fifth order polynomial extrapolation of the numerical solutions just obtained in the vicinity of these two voltages. The extrapolations were made twice, each time with a new set of quasi-Fermi potentials and electrostatic potentials computed at the extrapolated maximum power voltage or open circuit voltage.

An illustration of the numerical procedure was given by Maes and Sah [16] who computed the d.c. dark I-V characteristics of gold diffused silicon diodes and by Chan and Sah who computed the d.c. dark I-V characteristics of zinc diffused silicon diodes recently [10]. The differences between these dark forward I-V calculations and the illuminated forward I-V calculations are the addition of the photocurrent generator and the I-V locus used in the calculation. The illuminated I-V locus of calculation was just described.

To compute the efficiency of silicon solar cells containing zinc, the following diode material and device properties were selected.

(1) Zinc concentration is assumed constant over the diode. This assumption may differ from practical situations where the high concentration of the phosphorus or boron diffusant in the diffused emitter or the back surface field layer may enhance or depress the solubility of zinc. The enhanced solubility will only slightly decrease the cell performance since the results, to be presented, show that base recombination dominates the cell performance for practical base lifetimes for 10^{11} to 10^{14} Zn/cm^3.

(2) Interband Auger recombination was included in the computation to give a more realistic situation when the zinc concentration was extremely low. However, no other base recombination other than zinc is included.

(3) Both the n+/p/p+ and p+/n/n+ back surface field cell structures are analyzed numerically. The thickness of the cell is taken as 250 μm. The

diffused emitter junction is located at 0.25 μm from the front surface and the diffused back surface field layer concentration drops to bulk dopant value at 1.0 μm from the back surface. Measured boron and diffusion profiles are fitted analytically and used here [17,18]. The phosphorus profile is fitted to $\exp(-X^6)$ due to its rather flat plateau and sharp drop off. The boron profile is fitted to $(1 - X^{2/3})$ again simulating a flat plateau and sharp drop off. The rather abrupt phosphorus profile increases emitter recombination and reduces the short circuit current by nearly 2 mA/cm^2 while the boron emitter profile reduces the short circuit current only about 0.2 mA/cm^2. Neither of these profiles have significant effects on the open circuit voltage which is determined mainly by recombination at the zinc centers in the base region. The profiles employed are given below.

$$N_{AA} - N_{DD} = C_0[1 - x^{2/3}/L_1] - C_B - C_L\exp[-(L-x)^6/L_2] \qquad (p+/n/n+)$$

$$N_{DD} - N_{AA} = C_0\exp[-x^6/L_1] \quad - C_B - C_L[1 - (L-x)^{2/3}/L_2] \qquad (n+/p/p+)$$

where L=250 μm and L_1 and L_2 are determined by the junction depth of 0.25 μm for the emitter and 1.0 μm for the back surface field. A value of 2.5×10^{20} cm^{-3} is used for both the front and back surface concentrations, C_0 and C_L. The bulk concentration is taken as 5×10^{14} cm^{-3}. For p-base or n+/p/p+ cells, this corresponds to a base resistivity of 25 ohm-cm. For n-base or p+/n/n+ cells, this corresponds to a base resistivity of 10 ohm-cm. An increase of the base doping concentration by 10 to 5×10^{15} cm^{-3} will increase the AM1 maximum efficiency by about 1% (from 16% to 17%).

(4) Antireflection coating is assumed to eliminate surface reflection completely. For a bare cell surface without antireflection coating, the short circuit current is reduced by about 36%.

(5) The AM1 solar spectral density tabulated by Thekaehara [19] at the

ambient condition of 20 mm H_2O and 3.4 mm O_3 with a total incident power of 88.92 mW/cm^2 is employed. This is somewhat smaller than the industrial standard of 100 mW/cm^2. The photocurrent generator located at position x_1 for the lump section located between x_1 and x_2 is given by

$$J_0(x_1) = q\int_{\lambda_0}^{\lambda_\infty} (\lambda/hc)P(0,\lambda)[e^{-\alpha x_1} - e^{-\alpha x_2}]d\lambda/(x_2-x_1)$$

where $P(0,\lambda)$ is the incident AM1 solar power spectral density ($W/m^2\mu$), λ the photon wavelength, h the Plank constant, c the velocity of light in air, λ_∞ the cut-off wavelength of silicon determined by the silicon absorption coefficient, α, and approximately given by $\lambda_\infty = hc/E_G$, and λ_0 the cut-off wave-length of the solar spectrum. This photocurrent generator gives the value averaged over the lump section whose thickness is (x_2-x_1). Such an average insures that computed short circuit current does not exceed the available photocurrent due to numerical inaccuracy.

(6) The silicon absorption coefficient as well as the reflection coefficient described in (4) were obtained by interpolation of the data given in the literature. The absorption coefficients were numerical interpolation of values read off enlarged figures of the data of McFarlan, et. al. [20] and Philipp and Taft [21]. The reflection coefficients were obtained similarly from the data of Philipp and Taft [21]. These are given in the table in the appendix. The four significant figures listed do not imply absolute accuracy but serve as a constant base for numerical comparison of the performance of different cell geometries and material properties.

(7) The properties of the silicon material used in this analysis are also given in the appendix. These include the intrinsic carrier density, n_i, which contains energy gap narrowing due to Debye screening by the high density of electrons or holes in the diffused layers, and the lattice (acoustical and optical or intervalley phonon) and impurity scattering limited mobilities.

4. PROJECTED AM1 PERFORMANCE

The open circuit voltage, short circuit current, fill factor and maximum efficiency at AM1 illumination were numerically obtained. The fill factor is about 0.8 and varies by 0.02 among the cases and hence are not displayed in figures while the other factors are all given graphically.

The maximum AM1 efficiencies are shown in Figure 2. Two of the four curves, 1a and 2a, contained interband Auger recombination while the other two did not. Curves 1 and 1a are for the n+/p/p+ cells and 2 and 2a are for the p+/n/n+ cells.

It is evident that the p+/n/n+ cell has a slightly higher efficiency than the n+/p/p+ cell when the Auger recombination is included. The small difference arises mainly from the interband Auger recombination in the p+ and n+ emitters. These results show that in order to have a cell efficiency of 17%, the zinc concentration must be less than about $4x10^{11}$ Zn/cm^3 in the p-base or n+/p/p+ cell and less than about $7x10^{11}$ Zn/cm^3 in the n-base or p+/n/n+ cell.

If the base dopant impurity concentration is increased by 10 to $5x10^{15}$ cm^{-3}, the maximum allowable zinc concentration is increased by a factor of about 2. Thus, for the p-base cell of $5x10^{15}$ Boron/cm^3 (3 ohm-cm), the maximum zinc concentration for 17% efficiency is about $8x10^{11}$ Zn/cm^3. For the n-base cell of $5x10^{15}$ Phosphorus/cm^3 (1 ohm-cm), the maximum zinc concentration for 17% efficiency is about $1.5x10^{12}$ Zn/cm^3.

The effects of zinc concentration on the open circuit voltage and short circuit current are shown in Figures 3 and 4. The open circuit voltage is not affected by the interband Auger recombination in the diffused emitter and has nearly the same values in p-base and n-base cells as shown in Figure 3. The Auger recombination in the emitter is not important unless the zinc

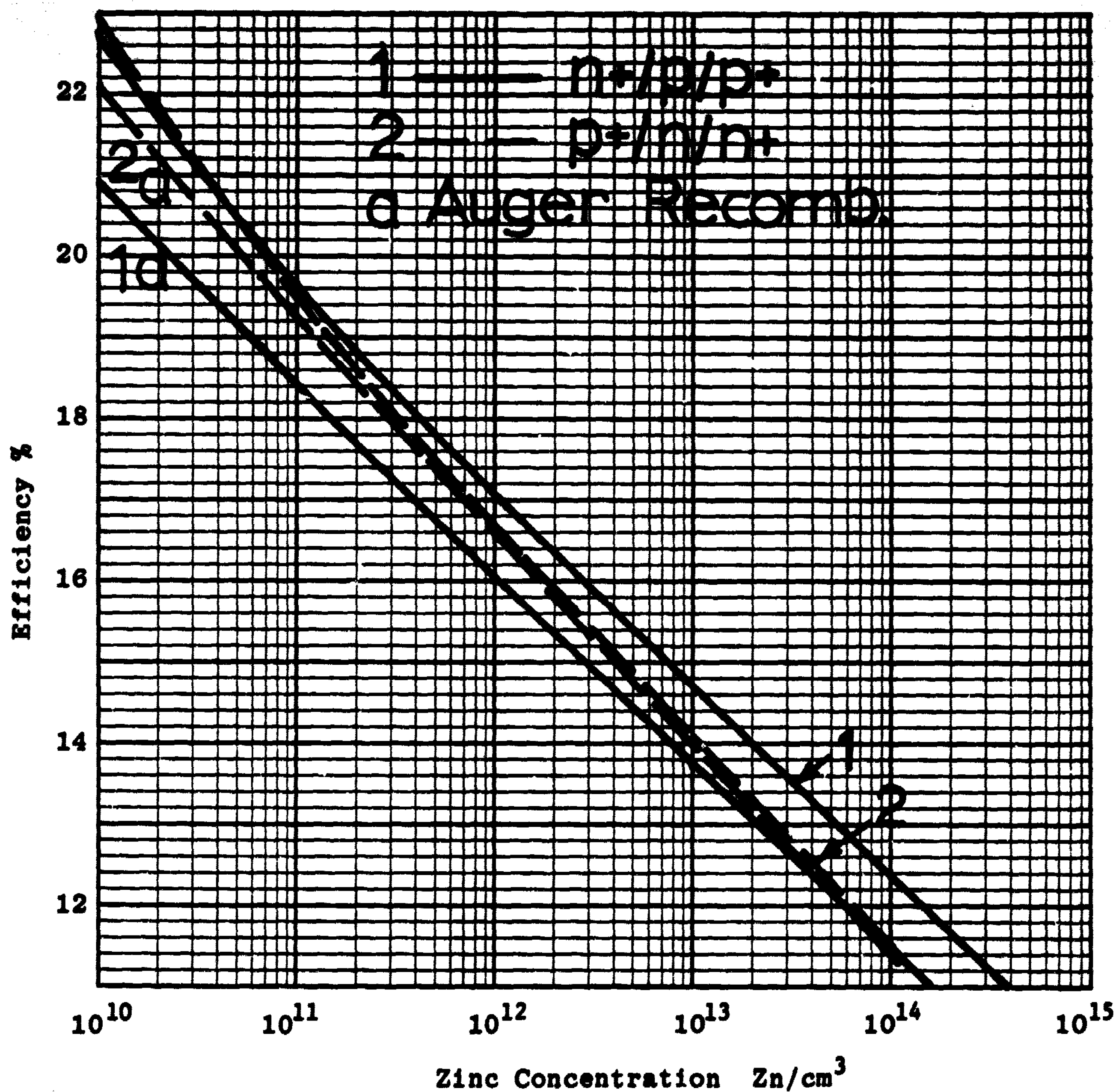

Figure 2 Theoretical AM1 efficiency as a function of Zn concentration at 296.6K for back surface field silicon solar cells with perfect antireflection coating. Curves 1a and 2a include interband Auger recombination. Curves 1 and 1a for n+/p/p+ and curves 2 and 2a for p+/n/n+ cells.

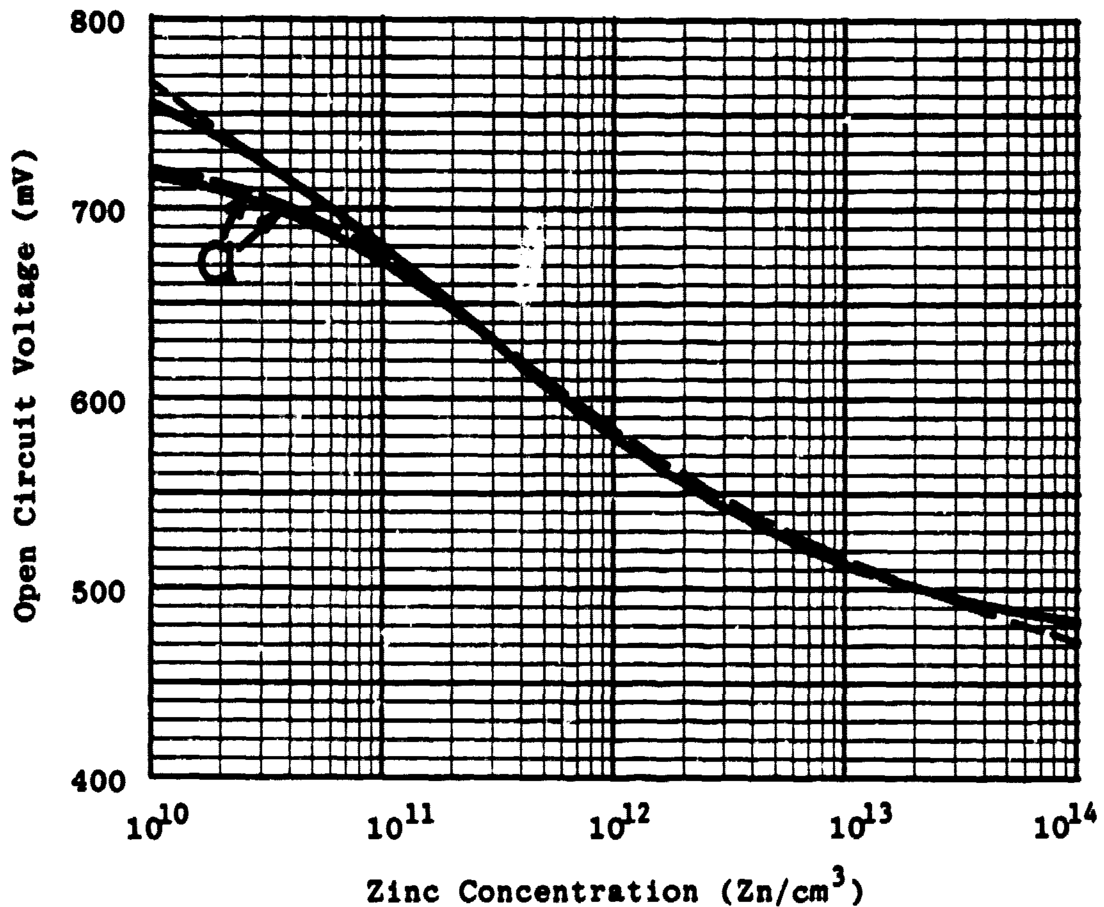

Figure 3 Theoretical AM1 open circuit voltage as a function of Zn concentration at 296.6K for back surface field silicon solar cells with perfect antireflection coating. Solid curves are for n+/p/p+ cells and dashed curves p+/n/n+ cells. Curves labeled a include interband Auger recombination.

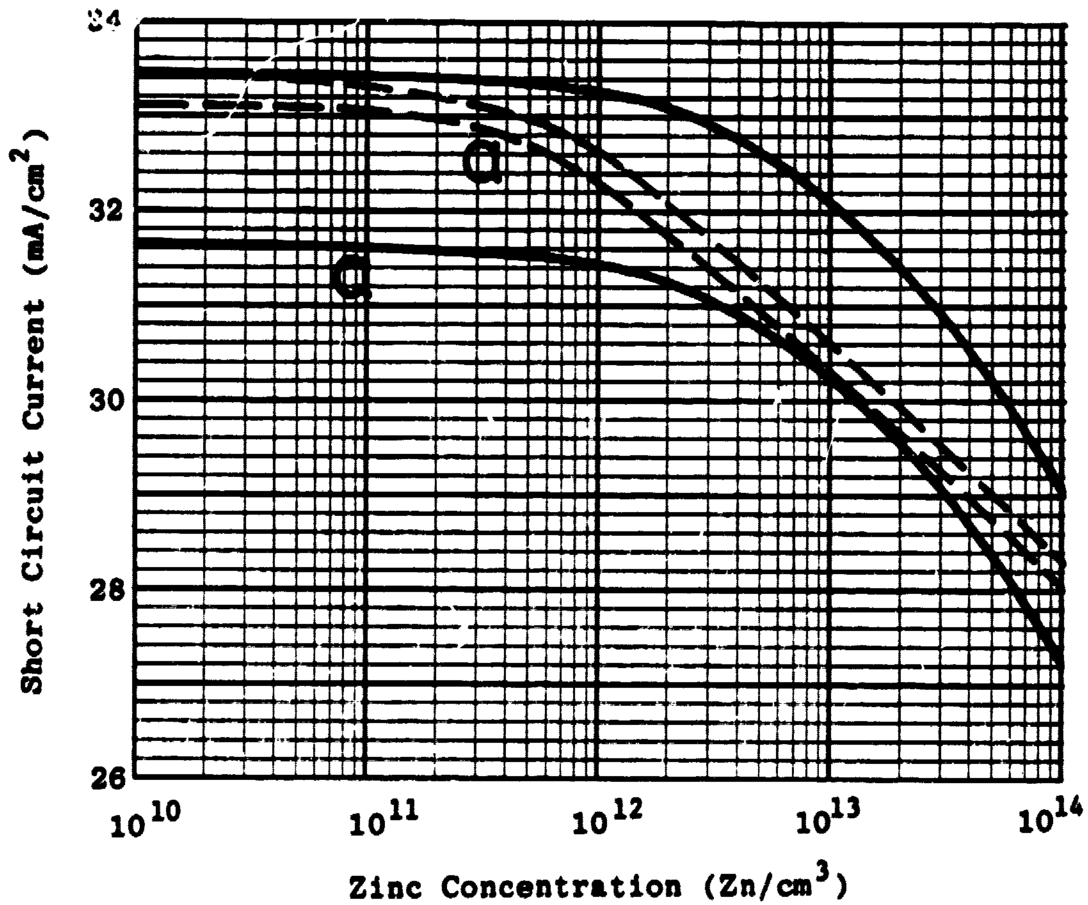

Figure 4 Theoretical AM1 short circuit current as a function of Zn concentration at 296.6K for back surface field silicon solar cells with perfect antireflection coating. Solid curves are for n+/p/p+ cells and dashed curves p+/n/n+ cells, Curves labeled a include interband Auger recombination.

concentration is less than 10^{11} Zn/cm^3 in the base. When it is greater than 10^{11} in the base, base recombination dominates the open circuit voltage.

The short circuit current at low zinc concentration or large base lifetime is mainly determined by emitter recombination as indicated by the four curves in Figure 4 for the short circuit current. Interband Auger recombination in the n+/p/p+ cells has a significant effect. It reduces the short-circuit current by about 2 mA/cm^2. This comes about from the high phosphorus concentration in the diffused emitter which is nearly constant until it reaches the junction where it drops off abruptly. Interband Auger recombination has a much smaller affect on the short circuit current in the p+/n/n+ cell, reducing it only by about 0.2 mA/cm^2. Reducing the surface concentration of the diffused emitter will reduce the interband Auger recombination loss. The results shown in Figure 4 indicate that the short circuit current begins to decrease due to base recombination when the zinc concentration is higher than about 10^{12} Zn/cm^3.

5. CONCLUSIONS

Numerical calculations using the exact one-dimensional circuit model show that zinc recombination centers reduce the performance of silicon solar cells significantly due to recombination of electrons and holes in the base region of the cells. The reduction is nearly the same for p+/n/n+ and n+/p/p+ cells. To get an AM1 efficiency of 17%, the zinc concentration in the base of the n-base cell must be less than $7x10^{11}$ Zn/cm^3 and in the p-base cell, less than $4x10^{11}$ Zn/cm^3 for a base dopant concentration of $5x10^{14}$ cm^{-3}. Increase in the base dopant concentration by a factor of 10 to $5x10^{15}$ cm^{-3} would increase the maximum allowable zinc concentration by a factor of two to maintain a 17% AM1 efficiency.

APPENDIX

In Table 2, the solar power spectral density, $P(W/m^2-\mu)$, is given as a function of photon wavelength, $\lambda(\mu)$, and energy $E(eV)$. The AM1 solar power spectral irradiance is obtained by Thekaekara [19] at the atmospheric condition of 20 mm H_2O and 3.4 mm O_3. Some numerical interpolation of Thekaekara's data is made in preparing the table.

The silicon absorption coefficient as a function of photon energy or wavelength is also tabulated in Table 2. The data are obtained by interpolation of the data given by MacFarlane, et. al. [20] near the threshold energy and by Philipp and Taft [21] in the higher energy range. Although values were read off enlarged pictures of the figures given by MacFarlane, et. al. and Philipp and Taft, the four significant figures given do not imply absolute accuracy but are used to provide a constant base for comparison of performance of different cell geometries and materials. The absorption tail does provide several tenths of mA/cm^2 of short circuit current due to its deep penetration. Thus, a constant set of values is essential to provide a constant base for comparison.

The surface reflection coefficient, $R(\lambda)$, and the transmission coefficient, $1 - R(\lambda)$, as a function photon wavelength or energy is also tabulated in Table 2. These values are obtained by interpolation of the published data of Philipp and Taft [21] whose figures were enlarged and the values visually read off and then least square fitted to a polynomial. The four significant figures given in the table again provide a constant base for comparison purposes and do not imply absolute accuracy.

In the current calculations presented in section 4, a perfect anti-reflection coating is assumed so that the reflection coefficient is assumed to be zero or the transmission coefficient is assumed to be unity.

Table 2 AM1 solar spectral irradiance, P, silicon absorption coefficient, α, and silicon surface reflection coefficient, R(λ), as a function of photon wave length, λ. 88.92 mW/cm^2. (part 1, 2900-6000A)

λ(μ)	E(eV)	$\alpha(cm^{-1})$	$P(W/m^2\mu)$	1-R(λ)
.2900D+00	.4275D+01	.2119D+07	.0000D+00	.3329D-00
.2950D+00	.4203D+01	.1868D+07	.0000D+00	.3881D-00
.3000D+00	.4133D+01	.168[illegible]+07	.4100D+01	.3881D-00
.3050D+00	.4065D+01	.15[illegible]+07	.1140D+02	.4065D-00
.3100D+00	.4000D+01	.14[illegible]07	.3050D+02	.4198D-00
.3150D+00	.3936D+01	.1344D+07	.7940D+02	.4285D-00
.3200D+00	.3875D+01	.1270D+07	.2026D+03	.4366D-00
.3250D+00	.3815D+01	.1204D+07	.2695D+03	.4430D-00
.3300D+00	.3757D+01	.1151D+07	.3316D+03	.4465D-00
.3350D+00	.3701D+01	.1121D+07	.3834D+03	.4470D-00
.3400D+00	.3647D+01	.1103D+07	.4313D+03	.4465D-00
.3450D+00	.3594D+01	.1089D+07	.4492D+03	.4412D-00
.3500D+00	.3543D+01	.1066D+07	.4805D+03	.4330D-00
.3550D+00	.3493D+01	.1050D+07	.4980D+03	.4250D-00
.3600D+00	.3444D+01	.1003D+07	.5137D+03	.4180D-00
.3650D+00	.3397D+01	.8838D+06	.5613D+03	.4136D-00
.3700D+00	.3351D+01	.6194D+06	.6035D+03	.4137D-00
.3750D+00	.3307D+01	.4419D+06	.6094D+03	.4220D-00
.3800D+00	.3263D+01	.2979D+06	.6080D+03	.4389D-00
.3850D+00	.3221D+01	.2044D+06	.6098D+03	.4575D-00
.3900D+00	.3179D+01	.1532D+06	.6239D+03	.4742D-00
.3950D+00	.3139D+01	.1242D+06	.6912D+03	.4900D-00
.4000D+00	.3100D+01	.9596D+05	.8499D+03	.5040D-00
.4050D+00	.3062D+01	.7453D+05	.9928D+03	.5150D-00
.4100D+00	.3024D+01	.6389D+05	.1074D+04	.5256D-00
.4150D+00	.2988D+01	.5903D+05	.1105D+04	.5355D-00
.4200D+00	.2952D+01	.5619D+05	.1104D+04	.5459D-00
.4250D+00	.2918D+01	.5341D+05	.1087D+04	.5540D-00
.4300D+00	.2884D+01	.4840D+05	.1068D+04	.5614D-00
.4350D+00	.2851D+01	.4111D+05	.1100D+04	.5685D-00
.4400D+00	.2818D+01	.3399D+05	.1216D+04	.5750D-00
.4450D+00	.2786D+01	.2901D+05	.1310D+04	.5806D-00
.4500D+00	.2755D+01	.2675D+05	.1388D+04	.5859D-00
.4550D+00	.2725D+01	.2454D+05	.1435D+04	.5912D-00
.4600D+00	.2696D+01	.2238D+05	.1452D+04	.5958D-00
.4650D+00	.2667D+01	.2026D+05	.1451D+04	.5997D-00
.4700D+00	.2638D+01	.1819D+05	.1451D+04	.6035D-00
.4750D+00	.2610D+01	.1616D+05	.1470D+04	.6066D-00
.4800D+00	.2583D+01	.1493D+05	.1503D+04	.6097D-00
.4850D+00	.2557D+01	.1419D+05	.1443D+04	.6125D-00
.4900D+00	.2531D+01	.1342D+05	.1435D+04	.6152D-00
.4950D+00	.2505D+01	.1265D+05	.1454D+04	.6176D-00
.5000D+00	.2480D+01	.1202D+05	.1451D+04	.6200D-00
.5050D+00	.2455D+01	.1143D+05	.1440D+04	.6220D-00
.5100D+00	.2431D+01	.1081D+05	.1417D+04	.6240D-00
.5150D+00	.2408D+01	.1020D+05	.1385D+04	.6262D-00
.5200D+00	.2385D+01	.9691D+04	.1390D+04	.6281D-00
.5250D+00	.2362D+01	.9237D+04	.1410D+04	.6300D-00
.5300D+00	.2340D+01	.8833D+04	.1407D+04	.6321D-00
.5350D+00	.2318D+01	.8483D+04	.1394D+04	.6338D-00
.5400D+00	.2296D+01	.8125D+04	.1372D+04	.6352D-00
.5450D+00	.2275D+01	.7704D+04	.1354D+04	.6372D-00
.5500D+00	.2254D+01	.7290D+04	.1337D+04	.6388D-00
.5550D+00	.2234D+01	.7010D+04	.1336D+04	.6400D-00
.5600D+00	.2214D+01	.6771D+04	.1319D+04	.6411D-00
.5650D+00	.2195D+01	.6525D+04	.1330D+04	.6426D-00
.5700D+00	.2175D+01	.6255D+04	.1338D+04	.6437D-00
.5750D+00	.2156D+01	.5991D+04	.1347D+04	.6448D-00
.5800D+00	.2138D+01	.5779D+04	.1347D+04	.6458D-00
.5850D+00	.2120D+01	.5596D+04	.1347D+04	.6469D-00
.5900D+00	.2102D+01	.5416D+04	.1341D+04	.6477D-00
.5950D+00	.2084D+01	.5208D+04	.1329D+04	.6486D-00
.6000D+00	.2067D+01	.4999D+04	.1320D+04	.6497D-00

Table 2 AM1 solar spectral irradiance, P, silicon absorption coefficient, α, and silicon surface reflection coefficient, R(λ), as a function of photon wave length, λ. 88.92 mW/cm^2. (part 2, 6000-12640A)

λ(μ)	E(eV)	$\alpha(cm^{-1})$	$P(W/m^2\mu)$	1-R(λ)
.6000D+00	.2067D+01	.4999D+04	.1320D+04	.6497D-00
.6050D+00	.2050D+01	.4795D+04	.1311D+04	.6503D-00
.6100D+00	.2033D+01	.4627D+04	.1308D+04	.6512D-00
.6200D+00	.2000D+01	.4300D+04	.1294D+04	.6529D-00
.6300D+00	.1968D+01	.3982D+04	.1281D+04	.6543D-00
.6400D+00	.1937D+01	.3675D+04	.1272D+04	.6559D-00
.6500D+00	.1908D+01	.3377D+04	.1257D+04	.6571D-00
.6600D+00	.1879D+01	.3130D+04	.1244D+04	.6587D-00
.6700D+00	.1851D+01	.2906D+04	.1227D+04	.6600D-00
.6800D+00	.1823D+01	.2714D+04	.1210D+04	.6607D-00
.6900D+00	.1797D+01	.2529D+04	.1196D+04	.6620D-00
.6980D+00	.1776D+01	.2385D+04	.1010D+04	.6632D-00
.7000D+00	.1771D+01	.2350D+04	.1175D+04	.6638D-00
.7100D+00	.1746D+01	.2179D+04	.1157D+04	.6648D-00
.7200D+00	.1722D+01	.2033D+04	.1135D+04	.6660D-00
.7280D+00	.1703D+01	.1920D+04	.1003D+04	.6670D-00
.7300D+00	.1699D+01	.1892D+04	.1118D+04	.6672D-00
.7400D+00	.1676D+01	.1754D+04	.1095D+04	.6679D-00
.7500D+00	.1653D+01	.1620D+04	.1077D+04	.6690D-00
.7620D+00	.1627D+01	.1464D+04	.7940D+03	.6701D-00
.7700D+00	.1610D+01	.1362D+04	.1039D+04	.6705D-00
.7800D+00	.1590D+01	.1259D+04	.1019D+04	.6710D-00
.7900D+00	.1570D+01	.1178D+04	.1000D+04	.6726D-00
.8000D+00	.1550D+01	.1100D+04	.9812D+03	.6735D-00
.8060D+00	.1538D+01	.1044D+04	.8744D+03	.6738D-00
.8250D+00	.1503D+01	.8744D+03	.9316D+03	.6746D-00
.8300D+00	.1494D+01	.8358D+03	.9218D+03	.6750D-00
.8350D+00	.1485D+01	.8000D+03	.9124D+03	.6752D-00
.8460D+00	.1466D+01	.7228D+03	.4762D+03	.6758D-00
.8600D+00	.1442D+01	.6306D+03	.5064D+03	.6766D-00
.8700D+00	.1425D+01	.5709D+03	.4538D+03	.6771D-00
.8750D+00	.1417D+01	.5416D+03	.4492D+03	.6774D-00
.8870D+00	.1398D+01	.4738D+03	.4486D+03	.6780D-00
.9000D+00	.1378D+01	.4132D+03	.4489D+03	.6784D-00
.9070D+00	.1367D+01	.3813D+03	.4552D+03	.6788D-00
.9150D+00	.1355D+01	.3455D+03	.4615D+03	.6791D-00
.9250D+00	.1341D+01	.3053D+03	.2790D+03	.6795D-00
.9300D+00	.1333D+01	.2866D+03	.2218D+03	.6797D-00
.9400D+00	.1319D+01	.2497D+03	.3134D+03	.6800D-00
.9500D+00	.1305D+01	.2136D+03	.2965D+03	.6805D-00
.9550D+00	.1298D+01	.1968D+03	.3211D+03	.6807D-00
.9650D+00	.1285D+01	.1699D+03	.3444D+03	.6810D-00
.9750D+00	.1272D+01	.1435D+03	.5769D+03	.6813D-00
.9850D+00	.1259D+01	.1177D+03	.5446D+03	.6813D-00
.1018D+01	.1218D+01	.5200D+02	.6175D+03	.6827D-00
.1082D+01	.1146D+01	.6568D+01	.5129D+03	.6842D-00
.1094D+01	.1133D+01	.4750D+01	.4641D+03	.6845D-00
.1098D+01	.1129D+01	.4210D+01	.5037D+03	.6847D-00
.1101D+01	.1126D+01	.3850D+01	.5048D+03	.6848D-00
.1128D+01	.1099D+01	.1600D+01	.1351D+03	.6850D-00
.1131D+01	.1096D+01	.1460D+01	.1522D+03	.6852D-00
.1137D+01	.1090D+01	.1150D+01	.1431D+03	.6853D-00
.1144D+01	.1084D+01	.8800D+00	.1912D+03	.6854D-00
.1147D+01	.1081D+01	.7600D+00	.1745D+03	.6855D-00
.1178D+01	.1053D+01	.6200D-01	.3993D+03	.6860D-00
.1189D+01	.1043D+01	.2500D-01	.4022D+03	.6861D-00
.1193D+01	.1039D+01	.1900D-01	.4240D+03	.6862D-00
.1222D+01	.1015D+01	.4000D-02	.3918D+03	.6866D-00
.1236D+01	.1003D+01	.2000D-02	.3908D+03	.6869D-00
.1264D+01	.9810D+01	.0000D-00	.3292D+03	.6873D-00

For reference purposes, the available photocurrent as a function of the total silicon solar cell thickness under the AM1 condition is computed. One pass is assumed, that is, there is complete transmission at the back interface. The result is tabulated below and serves as a guide for a quick estimate of the maximum possible short circuit current for a given cell thickness. Higher values of short circuit current for thin cells than the tabulated values are possible if appreciable reflection occurs at the back interface, giving rise to multiple internal reflections and absorptions.

TABLE 3

MAXIMUM AVAILABLE PHOTOCURRENT AS A FUNCTION OF THE THICKNESS OF THE SILICON SOLAR CELLS

THICKNESS (μm)	AVAILABLE PHOTOCURRENT (mA/cm^2)
0.1	3.1318
0.2	4.7755
0.5	8.1773
1.0	11.812
2.0	16.219
5.0	22.296
10.0	26.208
20.0	29.088
50.0	31.491
100.0	32.772
150.0	33.438
200.0	33.880
250.0	34.198
300.0	34.353
400.0	34.826
500.0	35.101
1000.0	35.943
2000.0	36.839
5000	37.702
10000	37.491
∞	40.853

The material properties required in the silicon solar cell performance calculations are the intrinsic carrier density and the mobilities of electrons and holes. A more sophisticated model would also require the energy levels of the shallow level dopant impurities (phosphorus and boron) in silicon as well as their dependences on their concentration. These impurity deionization and impurity banding effects are not included since reliable theoretical models and experimental data are not available. Their inclusion will only slightly change the results.

The intrinsic carrier concentration is computed from

$$n_i = 2.51\text{x}10^{19}(m^*/m)^{3/2}(T/300)^{3/2}\ \exp(-E_G/2kT)$$

where the effective mass and the energy gap are given by

$$m^*/m = (m_N m_P/m^2)^{1/2} = 0.81577$$
$$+ 3.4353\text{x}10^{-3}[1 - (T/437.65) + (T/814.2)^2 + (T/1356)^3]T$$
$$E_G = 1.2080 - 2.800\text{x}10^{-4} + DE_G \ \text{(eV)}$$
$$DE_G = - q^2/4\pi\varepsilon(L_D+a) = - 1.2206374/(L_D+a) \quad \text{(eV/A)}$$
$$L_D = \sqrt{\varepsilon kT/q^2(N+P)}$$
$$a = [3/4\pi(N+P)]^{1/3}$$
$$\varepsilon = 11.8\text{x}8.85419\text{x}10^{-14}\ \text{F/cm}$$
$$q = 1.602192\text{x}10^{-19}\ \text{C}$$
$$k = 8.617087\text{x}10^{-5}\ \text{V/K}$$

Debye screening which reduces the energy gap is given by DE_G above. This expression is consistent with that previously used by Morin and Maita and attributed to Herring [22] but differs from those by recent authors based on less physical derivations. Debye screening is the only mechanism which can give a true energy gap narrowing. Other mechanisms, such as the random position distribution of impurity and host atoms, can give apparent energy gap narrowing known as band tail states. However, these tail states are localized or partially localized low mobility or zero mobility states and they cannot be included in

n_i which are carriers in the band with high mobilities. Energy gap narrowing is not included in this calculation, however, its effect is only important in the emitter region which has a concentration of majority carriers. Since emitter recombination is not the dominant factor (base recombination is) on the efficiency of zinc doped slicon solar cells, the inclusion of energy gap narrowing will reduce the performance only very slightly. This would not be the case if the base dopant impurity concentration is increased substantially, for example, to 10^{17} cm^{-3} or above.

The mobilities for majority and minority carriers are assumed to be equal and simple analytical fits are made to the experimental data. For AM1 operation, the current density is sufficiently low that even a factor of two change of mobility would not significantly affect the computed results. The mobility fits given below, however, are better than 10%. The scattering by the lattice vibrations (acoustical and optical or intervalley phonons) and by ionized impurities are taken into account but the scattering by dislocations and neutral impurities are not included whose effects are expected to be small. The three scattering mechanisms are combined using the simple Matthiessen's rule

$$\mu^{-1} = \mu_A^{-1} + \mu_R^{-1} + \mu_I^{-1}$$

which give excellent fits to the published experimental data. More elaborate formulae based on complicated theoretical models do not justify the additional computation time required compared with this simple Mathiessen model. The three contributions are:

$$\mu_A = 2.18\text{x}10^7 T^{-1.5} \quad (cm^2/V\text{-}s) \qquad \text{Electrons}$$

$$= 1.30\text{x}10^7 T^{-1.5} \qquad \text{Holes}$$

$$\mu_R = 1.22\text{x}10^{11} T^{-3.13} \qquad \text{Electrons}$$

$$= 6.64\text{x}10^{10} T^{-3.25} \qquad \text{Holes}$$

$$\mu_I = 90[1 + (2.0\text{x}10^{18}/C_I)(T/300)] \qquad \text{Electrons}$$

$$= 45[1 + (1.2\text{x}10^{18}/C_I)(T/300)] \qquad \text{Holes}$$

In the impurity scattering mobility formulae, the total ionized impurity concentration, C_I, includes both the ionized shallow dopant impurities and the ionized deep level recombination centers, such as zinc in this case:

$$C_I(x) = N_{AA}(x) + N_{DD}(x) + N_T(x)$$

where for zinc, $N_T(x) = N_1 + 2N_2$, where N_1 is the concentration of the singly charged zinc center and N_2 is the concentration of the doubly charged zinc center.

The numerical constants given in these mobility formulae were obtained by fitting the Mathiessen's rule to published experimental data of nearly pure silicon to heavily doped silicon (10^{10} to 10^{20} impurity ions/cm^3) in the temperature range of 4.2K to 600K. These fits are as good as those using more complicated theoretical formulae in recent publications.

REFERENCES

1. J. M. Blocher, Jr. and M. F. Browning
Evaluation of selected chemical processes for production of low-cost silicon, DOE/JPL 964339-79/15, August 15, 1979

2. C. S. Fuller and F. J. Morin
Diffusion and electrical behavior of zinc in silicon
Physical Review v105, 379-384, January 15, 1957

3. R. O. Carlson
Double acceptor behavior of zinc in silicon
Physical Review v108, 1390-1393, December 15, 1957

4. John M. Herman III and C. T. Sah
Thermal ionization rates and energies of holes at the double acceptor zinc centers in silicon
Physical Status Solidi (a) v14, 405-415, December 16, 1972

5. John M. Herman and C. T. Sah
Thermal capture of electrons and holes at zinc centers in silicon
Solid-State Electronics, v16, 1133-1139, October 1, 1973

6. C. T. Sah
Bulk and interface imperfections in semiconductors
Solid-State Electronics v19, 975-990, December 1, 1976

7. C. T. Sah
Detection of recombination centers in solar cells from junction capacitance transients
IEEE Transaction on Electron Devices, vED-24, 410-419, April 1977

8. C. T. Sah
Detection of defect and impurity centers in semiconductor by steady-state and transient junction capacitance and current techniques
Semiconductor Silicon, v77-2, 868-893, May 1977. The Electrochemical Society, Princeton, N.J.

9. C. T. Sah, et. al.
Thermally stimulated capacitance (TSCAP) in p-n junctions
Applied Physics Letters, v20, 193-195, March 1, 1972

   C. T. Sah and J. W. Walker
   Thermally stimulated capacitance for shallow majority-carrier traps
   Applied Physics Letters, v22, 384-385, April 15, 1973

   C. T. Sah, et. al.
   Junction edge region thermally stimulated capacitance (TSCAP) of n-Si doped with phosphorus and bismuth
   Applied Physics Letters, v25, 523-524, November 1, 1974

10. C. H. Chan and C. T. Sah
Experimental and theoretical studies of I-V characteristics of zinc-doped silicon p-n junctions using the exact DC circuit model
IEEE Transaction on Electron Devices, vED-26, 924-936, June 1979

C. H. Chan and C. T. Sah
Computer-aided study of steady-state carrier lifetimes under arbitrary injection conditions
Solid-State Electronics, v22, 921-926, November 1979

11. C. T. Sah and W. Shockley
Electron-hole recombination statistics in semiconductors through flaws with many charge conditions
Physical Review v109, 1103-1115, February 15, 1958

12. R. H. Kingston
Switching time in junction diodes and junction transistors
Proceeding of IRE, v42, 829-836, 1954

Paul E. Gray, David DeWitt and A. R. Boothroyd
PHYSICAL ELECTRONICS AND CIRCUIT MODELS OF TRANSISTORS
Chapter 5, Time-dependent performance of the junction diode
John Wiley and Sons, Inc. New York, 1962

13. C. T. Sah
The equivalent circuit model in solid-state electronics-Part II:
The multiple energy level impurity centers.
Procedding IEEE, v55, 672-684, May 1967.

14. C. T. Sah and F. A. Lindolm
Carrier generation, recombination, trapping and transport in semiconductors with position-dependent composition
IEEE Transaction on Electron Devices, vED-24, 358-362, April 1977

15. C. T. Sah
Equivalent circuit models in semiconductor transport for thermal, optical, Auger-impact and tunneling recombination-generation-trapping processes
Physical Status Solidi, (a) v7, 541-559, October 16, 1971

16. Herman Maes and C. T. Sah
Application of the equivalent circuit model for semiconductors to the study of Au-doped p-n junctions under forward bias
IEEE Transaction on Electron Devices, vED24, 1131-1143, October 1976

17. Richard B. Fair
Analysis of phosphorus-diffused layers in silicon
J. Electrochemical Society, v125, 323-327, February 1, 1978

18. Richard B. Fair
Boron diffusion in silicon - concentration and orientation dependence, background effects and profile estimation
J. Electrochemical Society, v122, 800-805, June 1, 1975

19. Matthews P. Thekaekara
Data on incident solar energy
Journal of Environmental Science, v17, 21-49, 1974

20. G. G. MacFarlane, T. P. McLean, J. E. Quarrington and V. Robert
Fine structure in the absorption-edge spectrum of Si
Physical Review, v111, 1245-1254, September 1, 1958

21. H. R. Philipp and E. A. Taft
Optical constants of silicon in the region of 1 to 10 eV
Physical Review v120, 37-38, October 1, 1960

22. F. J. Morin and J. P. Maita
Conductivity and Hall effects in the intrinsic range of germanium
Physical Review v94, 1525-1529, June 15, 1954